Deceleration of Accelerator-Produced and In-Trap Electron Cooling of Highly Charged Ions

S. Rausch,[1,2,*] Z. Andelkovic,[3] S. Fedotova,[3] W. Geithner,[3] F. Herfurth,[3] M. Horst,[1,2] J. Ködel,[1] K. Mohr,[1,2] D. Neidherr,[3] W. Nörtershäuser,[1,2] N. Stallkamp,[3,4] S. Trotsenko,[3] G. Vorobjev,[3] and D. Zisis[1,2]

[1]*Institut für Kernphysik, Technische Universität Darmstadt, Schloßgartenstrasse 9, Darmstadt, Germany*
[2]*Helmholtz Akademie Hessen für FAIR HFHF, GSI Helmholtzzentrum für Schwerionenforschung GmbH, Planckstrasse 1, Darmstadt, Germany*
[3]*GSI Helmholtzzentrum für Schwerionenforschung GmbH, Planckstrasse 1, Darmstadt, Germany*
[4]*Institut für Kernphysik, JWGU Frankfurt, Max-von-Laue-Strasse 9, Frankfurt am Main, Germany*

(Received 11 July 2025; accepted 13 May 2026; published 29 July 2026)

The most efficient and most versatile technique for producing highly charged ions (HCI) with high atomic numbers is electron stripping in-flight at high kinetic energies. While this requires relativistic velocities, many experiments call for trapped or at least slowly moving ions. For example, studies of fundamental interactions would significantly improve in precision when performed in an ion trap while studies on slow HCI for material science are not yet feasible due to the lack of availability. The goal of the HITRAP project at the GSI Helmholtzzentrum für Schwerionenforschung GmbH is to decelerate accelerator-produced heavy HCI and prepare them in a Penning trap via electron cooling for subsequent experiments. We present the trapping of accelerator-produced HCI. Fully stripped $^{36}Ar^{18+}$ were decelerated from the production energy of 45 MeV/u to 6 keV/u followed by trapping in the HITRAP Cooling Trap for the duration of several seconds. The Cooling Trap is a nested Penning trap that allows for the simultaneous storage of HCI ions with a cold electron plasma. It was commissioned with HCI from a local electron beam ion source, which led to the first observation of electron cooling of highly charged ions in a Penning trap, marking a significant advancement in the field. These developments constitute a major step toward a worldwide unique facility with unparalleled capabilities in heavy-ion research and already enable the first experimental studies at HITRAP.

DOI: 10.1103/961c-j3p5

Subject Areas: Atomic and Molecular Physics, Nuclear Physics

I. INTRODUCTION

The study of highly charged ions (HCI) opens the door to a broad spectrum of applications and fields. They naturally occur only in the most extreme environments of the Universe, such as stellar interiors or supernovae. Thus, HCI are of particular interest in astronomy and astrophysics [1–3]. In recent years, the application of HCI for high-accuracy optical clocks has attracted the attention of the metrology community, with objectives including the potential discovery of a time-dependent variation of the fine structure constant α [4–6]. From a theoretical standpoint, the most stringent tests of quantum electrodynamics (QED) are expected from precision measurements of the properties of heavy HCI [7–9].

QED is widely regarded as the most precisely experimentally verified theory. This is particularly evident for simple systems, such as a free electron, where the observed g-factor is in agreement with the theoretical prediction within its relative uncertainty of $< 10^{-12}$ [10], and for light and medium heavy HCI [11–15]. For a bound electron, the g-factor can be represented by a series expansion in α and is given by

$$g_J = 2\left(1 + D_2[\alpha Z]\left(\frac{\alpha Z}{\pi}\right) + D_4[\alpha Z]\left(\frac{\alpha Z}{\pi}\right)^2 + \cdots + a_{\mathrm{nuc}}\right). \tag{1}$$

As both the expansion factor and the coefficients D_i scale with the atomic number Z, the theoretical prediction of the bound electron g-factor becomes increasingly difficult for heavier ions. The corrections for a finite nucleus are incorporated by the contribution a_{nuc} [16].

The experimental determination of the g-factor is typically accomplished through measurements based on the continuous Stern-Gerlach effect, which define its value as

*Contact author: s.rausch@gsi.de

$$g_J = 2\frac{Q}{e}\frac{m_e}{M}\frac{\omega_L}{\omega_c}, \tag{2}$$

with the charges e and Q of the electron and ion, and their respective masses m_e and M [17]. The ratio of the electron's Larmor frequency ω_L and the ion's cyclotron frequency ω_c can be measured in a Penning trap with particular high precision. Such measurements have been performed with extreme accuracy for light and medium-heavy highly charged ions such as $^{12}C^{5+}$ [11], $^{28}Si^{13+}$ [16], or even $^{118}Sn^{49+}$ [15], where the latter achieved a relative uncertainty of $< 10^{-9}$ with the results being in good agreement with the predicted values. This level of accuracy even allows probing for third-order two-loop QED effects and is sensitive to the influence of the nonzero nuclear size [18].

Additional nonlinear effects are expected for the heaviest nuclei since the electric field experienced by a $1s_{1/2}$ electron in hydrogenlike uranium approaches the Schwinger limit for spontaneous electron-positron pair production [19,20]. Consequently, precision measurements with heavy nuclei would allow for the most stringent test of QED to date. However, the required precision has not yet been achieved experimentally for HCI beyond tin, primarily due to the nonavailability of cold trapped ions of these species.

While the measurements for light- and medium-mass ions are based on the determination of motional frequencies in a Penning trap, that of the g-factor of the electron in hydrogenlike bismuth $^{209}Bi^{82+}$, for example, is currently derived from the lifetime of the ground state's upper hyperfine level measured in a storage ring [21]. This method results in a relative uncertainty of 10^{-3}, while theoretical predictions are available at a precision better than 10^{-6}, only limited by the higher complexity of the calculations for high-Z ions [22,23]. Similarly, the hyperfine splittings in the $1s$ and $2s$ states of hydrogenlike Bi^{82+} and lithiumlike Bi^{80+}, respectively, are considered to be a sensitive test of QED in the strongest magnetic fields available in the laboratory [24] and have been measured by laser spectroscopy at the experimental storage ring (ESR) to an accuracy of approximately 10^{-5} [25–27]. Also in these cases, measurements on cold ions stored in a Penning or Paul trap would boost experimental accuracy by several orders of magnitude and, thus, allow for much more conclusive tests of QED. Corresponding experiments under commissioning at HITRAP [28–31] require varying amounts from single to several 1000 ions.

While the discussion was so far focused on the application of heavy HCI in the study of fundamental interactions, we note that there are other fields interested in trapped or slow ions of these species. For example, the effect of a slowly approaching HCI with its enormous potential energy when approaching a surface is being studied in material science [32]. Indeed, this was the subject of the very first user beamtime carried out at HITRAP. Moreover, the formation of hollow atoms [33], strong-field atomic collisions [34], and astrophysical plasma [3] can be studied.

To date, the existing production methods for heavy HCI prevent their usage for all these kinds of investigations. While light and medium-heavy ions can be produced in large quantities within laboratory-sized ion sources like electron beam ion traps (EBITs) [35–38] or electron cyclotron resonance (ECR) [39,40] sources, heavy HCI can be produced in large numbers only by in-flight electron stripping at high kinetic energies in accelerator facilities.

These large quantities are essential for many of the abovementioned experiments. For example, surface ionization studies require the impingement in the order of 10^8 ions per cm^2 onto the target [41]. Also for the formation of heavy-ion plasmas or fluorescence laser spectroscopy in a Penning trap, single ions are not sufficient [42]. While bare uranium ions have been produced in small amounts in an EBIT [43], not even single ions of these heavy highly charged species have so far been extracted from the production environment that is hostile to precision experiments.

The approach of in-flight electron stripping is employed at the GSI Helmholtzzentrum für Schwerionenforschung GmbH, a heavy-ion research facility located in Germany. Following the production at low charge states in an ion source, the ions are accelerated by the universal linear accelerator (UNILAC) and the heavy-ion synchrotron SIS18 to energies of several hundreds of megaelectronvolts per nucleon (MeV/u). Thereafter, the ions are directed onto a thin stripper foil to remove the last remaining electrons through electron impact ionization [44]. It is not feasible to capture ions at these energies in a Penning trap, as this process would require static capture voltages in the MV regime. This limitation is addressed by the HITRAP project [28].

Here we report on the most recent commissioning experiments at HITRAP that resulted in significant advancements toward the completion of the HITRAP facility and the feasibility of the first experimental studies. Before discussing the results, we provide a description of the experimental setup of HITRAP and the relevant GSI accelerator facilities. The results of the commissioning process can be divided into two categories which are presented in Secs. III and IV. First, the recommissioning and additional characterizations of the two rf structures during a beamtime with bare argon ions is presented. This beamtime also ultimately led to the capture of accelerator-produced HCI in a Penning trap, the first of two major milestones discussed in Sec. III. The second major advancement constitutes the first evidence of electron cooling of highly charged ions in a Penning trap. Finally, the next steps in the commissioning process of HITRAP will be presented.

II. HITRAP FACILITY

The goal of the HITRAP project is to provide cold bunches of heavy, highly charged ions at rest for precision experiments. While the scope of the facility is focused on the provision of stable ion species, we also note that HITRAP will be able to provide radioactive isotopes as long as they are sufficiently long-lived (> 10 s). To this end, following the production by in-flight stripping, the ions are first stored in the experimental storage ring (ESR) before they are delivered to the HITRAP facility. The injection energy into the ESR depends at this point on the intended ion species, in particular on the binding energy of the last electron to be stripped. Lighter ions require less kinetic energy during the production process, whereas heavier ions arrive at the ESR with a maximum energy of up to 550 MeV/u. For the heavier ions, the beam properties feature a very large longitudinal emittance which requires the combined application of stochastic cooling at 400 MeV/u followed by a period of electron cooling [45]. The cooled beam can then be decelerated by continuously decreasing the frequency of the rf cavities, thereby reducing the kinetic energy of the ion beam. At an energy of 30 MeV/u the deceleration process is paused for an intermediate cooling period with the electron cooler. This is to restore the beam quality and reduce the rate of ion loss. During the second deceleration period, the ion energy is further reduced down to the acceptance energy of the first cavity of the HITRAP facility, which is 4.02(1) MeV/u [46]. Following a final brief cooling cycle with the electron cooler, the ions are extracted toward HITRAP. Further details on the ESR and its cooling and deceleration methods can be found in Refs. [45,47].

A. Linear decelerator

The centerpiece of the HITRAP facility is, next to the Cooling Trap which will be discussed in the next section in greater detail, a two-stage linear decelerator. A schematic representation of this decelerator is provided in Fig. 1. Ions arriving from the ESR are initially bunched by a double drift bunching system (DDB). The first of the two bunchers divides the incoming ion bunch into 10-ns-long microbunches to meet the longitudinal acceptance of the subsequent deceleration units [48]. As the efficiency of a single buncher is limited, the DDB comprises a second buncher that is spatially separated from the first one and operated at twice the frequency. This second buncher refines the original bunches, allowing for a theoretical bunching efficiency of approximately 60% [49].

Subsequent to the DDB is the primary deceleration stage of HITRAP, a 2.7-m-long interdigital H-type (IH) structure. In contrast to the more common use as an accelerator, the 26 drift tubes of this linear decelerator become increasingly shorter, allowing for a reduction of ion velocities. The unit requires up to 180 kW of rf power, depending on the ion species, in order to allow for the deceleration of the incoming ions from 4.02 MeV/u down to 0.49 MeV/u [50]. As the deceleration efficiency is predominantly determined by the bunching efficiency of the DDB, a theoretical limit of approximately 60% of the ions can be successfully decelerated to the design energy.

After the first deceleration step in the IH structure, a third buncher is available before the ions are injected into the next stage. This small spiral bunching unit can be employed to reshape the bunches and to make minor adjustments to the kinetic energy to meet the acceptance of the cavity. The following radio frequency quadrupole (RFQ) subsequently decelerates the ions from 0.49 MeV/u down to about 6 keV/u with a typical deceleration efficiency of 60%. The RFQ requires a peak power of up to 80 kW and accepts an energy range of (485 ± 10) keV/u. Measurements on a test setup and simulations predict challenging beam properties for the fully decelerated beam with the ion energy distributed between 6 and 7 keV/u and a transverse emittance of up to 100π mm mrad [51–54].

To transport this beam further along the beamline, a dedicated low-energy beamline has been designed to connect the linear decelerator with the Cooling Trap, the final stage of the HITRAP facility. This 2-m-long beamline section is equipped with six electrostatic einzel lenses operated with voltages of up to ± 65 kV, and four additional electrostatic steerers. Simulations suggest that the maximum transport efficiency of ions from the RFQ through this beamline is also approximately 60%. The

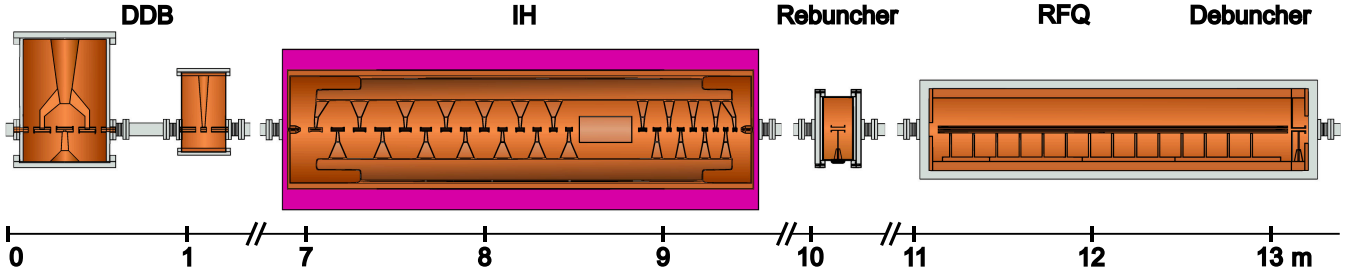

FIG. 1. Schematic overview of the HITRAP decelerator line consisting of a double drift buncher (DDB), an interdigital H-type (IH) structure, a rebuncher, and a radio frequency quadrupole (RFQ) with a debuncher on the exit side. To improve clarity, the beam-guiding elements between the rf cavities are omitted.

total deceleration and transport efficiency of the decelerator up until the end of the low-energy beamline can be up to 20%. Assuming 1×10^7 HCI coming from the ESR, a maximum of 2×10^6 can reach the end of the decelerator line.

In addition to the transport of the ion beam, this beamline section is also responsible for the separation of the vacuum sections. While the residual gas pressure inside the RFQ is of the order of only 10^{-7} mbar, the vacuum next to the ion trap is required to be below 1×10^{-9} mbar to achieve suitable conditions inside the trap for the storage of highly charged ions for several seconds [53]. This is accomplished by a combination of a pumping barrier of 8-mm diameter with two ion getter pumps, two turbo-molecular pumps, and a nonevaporable getter pump.

B. HITRAP Cooling Trap

The third and final stage of the HITRAP decelerator line is the Cooling Trap. As the beam properties that result from deceleration in the IH structure and RFQ prevent an efficient transport toward subsequent experimental setups, prior cooling of the ion bunch is imperative. This will significantly increase the transport efficiency and is also beneficial for precision experiments that require a cold ion bunch.

To address the challenge of cooling a wide range of ion species at high charge states and with a broad energy distribution, the only viable cooling technique is sympathetic cooling with a non-neutral plasma. At HITRAP, the special case of electron cooling was selected as the most suitable approach. This method involves the simultaneous storage of ions with a cold plasma of electrons within the same volume. The ions can then transfer their kinetic energy to the electrons via Coulomb interaction. In the magnetic field of a Penning trap, the electrons continuously radiate off their kinetic energy via synchrotron radiation. First applications of this technique included the cooling of antiprotons [55] and protons [56]. Only recently, the cooling of heavier, singly charged ions has been achieved [57].

In order to trap electrons simultaneously with ions of opposite charge in a Penning trap, a so-called nested-trap potential must be employed, as illustrated in Fig. 2. In this configuration, the electrons are confined in the trap center by the negative potentials, while the positive potentials capture the ions. The required flexibility in shaping the potential of the Penning trap is achieved with the electrode configuration depicted in Fig. 3. A more detailed description of the trap design can be found in Ref. [58]. To allow for the capture of the elongated ion bunches with high kinetic energy, that are expected to arrive at the Cooling Trap from the linear decelerator, the design of the electrode structure has to fulfill several uncommon requirements. Specifically, the two long end cap electrodes are deliberately extended to provide an effective trap length between

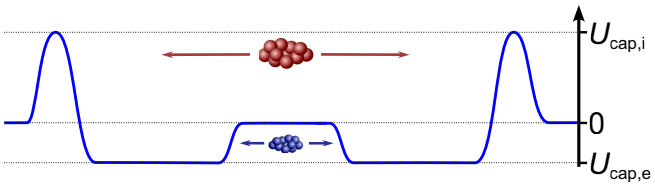

FIG. 2. Shape of a nested-trap potential that allows for the simultaneous storage of oppositely charged particles. In the case of electron cooling, the ions (red) are confined by positive capture potentials $U_{cap,i}$ while the electrons are confined in the center by negative potentials $U_{cap,e}$.

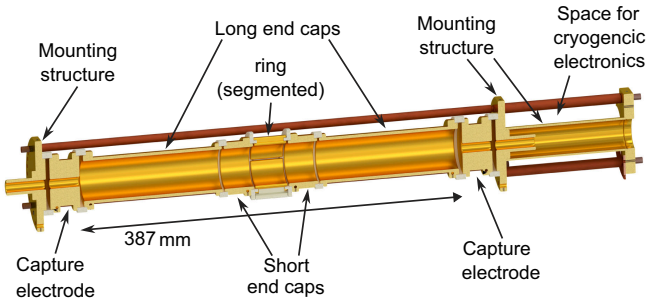

FIG. 3. Sectional view of the Penning trap inside the HITRAP Cooling Trap. The trap length between the two capture electrodes is 387 mm. The three central electrodes form a mechanically compensated trap, which allows for the production of a harmonic potential between the two short end cap electrodes.

the capture electrode of 38.7 cm. In addition, the electrical configuration of the setup must be capable of capturing ions from the linear decelerator with a kinetic energy per charge of up to 20 keV/q. To address this challenge, the entire apparatus can be biased with a potential of up to 12.5 kV, thereby effectively decelerating the ions upon their injection into the trap. Furthermore, the capture electrodes can be switched to a maximum potential of 10 kV to provide a maximum effective capture potential of 22.5 kV with respect to ground. Two high-power solid-state switches connected to the capture electrodes allow for fast potential modifications with a transition time of approximately 100 ns.

The Penning trap setup is completed by a superconducting magnet that radially confines the ions with a field strength of up to 6 T. To achieve necessary conditions for superconductivity, the magnet is cooled by a two-stage cold head cryocooler to a temperature of approximately 4 K. The cold head also functions to cool the bore to cryogenic temperatures. As a consequence, any residual gas particles will freeze to the surface of the vacuum tube, thereby significantly increasing the vacuum conditions inside the Penning trap. With this cryogenic pump, a residual gas pressure in the order of 10^{-13} mbar can be expected, which enables the storage of heavy, highly charged ions over an extended period of time.

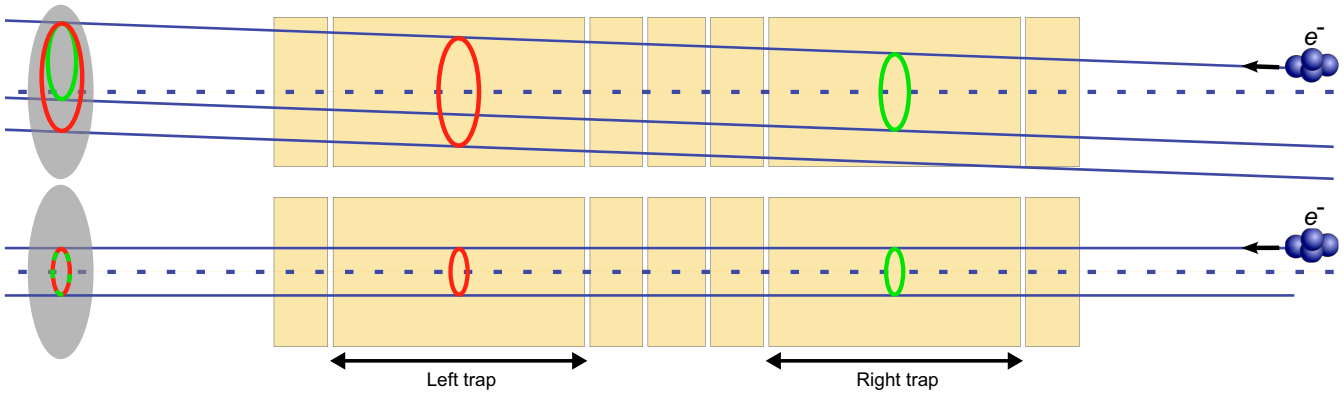

FIG. 4. Schematic representation of the technique employed to align the trap setup. The magnetic field is represented by the solid blue lines and the dashed lines indicate the trap's symmetry axis. Electrons are injected and captured in two distinct regions of the trap. For a misalignment between the electric and magnetic fields (top frame), the magnetron radius is contingent on the electrons' position within the trap. Conversely, for a perfectly aligned setup (bottom frame), the magnetron motion is independent of the electrons' position. The magnetron radius can be visualized by extracting the electrons at various phases of their magnetron motion, thus mapping the motion on a fluorescence screen which can be optically observed by a camera.

For the intended application of electron cooling, a cold plasma of electrons must be stored in the trap. Simulations suggest that a plasma of at least 10^9 electrons is required to enable effective electron cooling in the Cooling Trap [59,60]. Electrons are provided by a small, pulsed photoionization source that is located in the proximity of the Cooling Trap. This source is operated by irradiating a p-doped GaAs photocathode with an intense flash of ultraviolet light [61]. The thereby released electrons are accelerated by a negative potential applied to the cathode and then guided toward the Cooling Trap with a magnetic field generated by copper coils, where they can be captured in the center of the trap. Active cooling of the electron plasma is not required, as the electrons are passively cooled via synchrotron cooling in the strong magnetic field of the trap. Both the source and the guiding coils are operated in a pulsed mode to use the beamline in rapid succession for ions and electrons. The source produces a few 10^9 electrons per shot, of which about 1×10^9 can be captured due to the longitudinal acceptance of the trap.

While this value fulfills the minimum requirements for electron cooling as predicted by simulations, it is also expected that higher numbers will increase the cooling power. To increase the number of stored electrons in the Penning trap, multiple injections can be captured successively. This is achieved by applying a positive potential to the central ring electrode. As the electrons constantly radiate off their kinetic energy, they eventually fall into the potential well and remain confined, even if the long end cap electrodes responsible for the initial capture are switched back to ground. This process is repeated to inject and capture additional bunches of electrons, thereby resulting in a stepwise increase in the number of stored electrons. Only when the space-charge limit of the positive potential well is approached, the gain from additional injections is compensated by the loss of electrons due to unstable trapping conditions. The maximum electron number is therefore limited only by the applied stacking potential.

Another important prerequisite for effective electron cooling is a well aligned setup, meaning perpendicularly oriented magnetic and electric fields. This will improve the trapping conditions and facilitate the overlap between ions and electrons. The alignment of the Penning trap can be quantified and improved with the help of stored electrons. The procedure, which was first proposed in Ref. [62], involves confining electrons in two distinct regions of the Penning trap. The electrons perform a radial motion, that is defined by the overlapping electric and magnetic fields, the magnetron motion. The radius of this motion is contingent on the electron's distance to the symmetry axis of the Penning trap. As the electrons follow the magnetic field lines upon injection, the magnetron radius will, for a misaligned setup, consequently also depend on their position in the trap. This effect is schematically illustrated in Fig. 4.

With this technique, the radius of the magnetron motion could be decreased by a factor of more than 50, while the angular misalignment was reduced to $< 1 \times 10^{-3}$ deg. The enhanced alignment of the setup not only allows for an improved overlap between ions and electrons for the application of electron cooling, but also substantially increases the density of the electron plasma, consequently leading to a higher cooling power.

III. RECOMMISSIONING OF THE DECELERATOR

The commissioning of the HITRAP decelerator first commenced with the beamtime in 2007. The initial deceleration in the IH structure was accomplished by late 2008, and the subsequent deceleration step in the RFQ first

succeeded in 2014 [54]. However, due to a shift in priorities toward the low-energy storage ring CRYRING@ESR, the commissioning process of HITRAP was suspended for a period of eight years, resuming in 2022 with the successful deceleration of $^{58}Ni^{28+}$ ions. The results presented in the following sections stem from a beamtime in April 2024, starting with the recommissioning of the first two stages of the linear decelerator.

For this beamtime bare $^{36}Ar^{18+}$ ions, a comparably light ion species, were chosen on purpose to simplify the production process and to shorten the deceleration period in the ESR. After production in an ECR ion source (ECRIS) at a low charge state, the ions are accelerated by the linear accelerator UNILAC to 11.4 MeV/u. At this point, the remaining electrons are removed by a gaseous stripper target before the heavy-ion synchrotron SIS18 accelerates the ions to 45 MeV/u to meet the acceptance of the transport line toward the ESR. In contrast to heavier elements, further ionization is not required after SIS18. Thereafter, the ions are ejected toward the ESR, where the initial deceleration step to approximately 4 MeV/u takes place. Because of the comparably low injection energy, only one deceleration step is needed in the ESR which increases the deceleration efficiency and also the repetition rate. After a final brief period of electron cooling, approximately 3×10^7 ions are extracted toward the HITRAP decelerator line. The total duration of this process, starting at the ion sources up until the arrival at HITRAP, is about 43 s. The primary limitations of this process are the deceleration and cooling periods in the ESR.

Upon arrival at the HITRAP decelerator, the beam is bunched by the DDB into microbunches to meet the longitudinal acceptance of the IH structure. Subsequently, the kinetic energy of the ions can be determined by a pair of phase probe detectors. This detector comprises two spatially separated ring pickups, and measuring the difference in time of flight of a single microbunch between these two detectors yields a kinetic energy of $E_{\mathrm{kin}} = (4021.5 \pm 3.5)$ keV/u. This result meets the energy acceptance of the IH structure, i.e., the first deceleration step at HITRAP.

A. IH structure

After the beam is carefully aligned through the cavity of the IH structure, the deceleration process can be initiated. The two crucial parameters for setting up the IH structure are the phase shift with respect to the DDB system and the power of the rf signal. While the phase shift is solely determined by the velocity of the beam, the power P_{in} is given by the required effective deceleration voltage U_{eff} which in turn is determined by the dimensionless mass-to-charge ratio m/q of the ion species via the relation

$$U_{\mathrm{eff}} = \frac{1}{e} \triangle E_{\mathrm{kin}} \frac{m}{q}. \tag{3}$$

For a deceleration from 4.02 MeV/u to the acceptance energy of the RFQ of 0.49 MeV/u, the difference in kinetic energy $\triangle E$ is 3.53 MeV/u. Together with the length of the cavity $l = 2.613$ m and its effective shunt resistance $Z_{\mathrm{eff}} = 220$ MΩ/m, the required rf input power P_{in} can then be calculated as

$$P_{\mathrm{in}} = \frac{U_{\mathrm{eff}}^2}{Z_{\mathrm{eff}} T l}. \tag{4}$$

The change of the rf field during the transfer of ions through a gap in the cavity is accounted for by the transit-time factor $T = 0.85$. For bare $^{36}Ar^{18+}$ ions, this results in an rf power requirement of 102 kW.

To quantize the deceleration efficiency of the IH structure, a one-shot energy analyzer based on magnetic separation is installed downstream the beamline. This detector consists of a permanent dipole magnet with a 0.1-mm slit and a field of 500 mT that deflects the ions depending on their kinetic energy. After deflection, the ions are detected by a micro channel plate (MCP) detector with a fluorescence screen, which can be observed with a CCD camera [63,64]. The configuration and basic functionality of the detector are displayed in Fig. 5.

An exemplary image captured with this detector is presented on the left-hand side of Fig. 6 with the projection of the signal onto the vertical axis on the right-hand side. The projection plots the signal intensity over its position relative to the signal's maximum. With a calibration of the detector the kinetic energy of the components can be extracted from their position on the screen. The topmost peak corresponds to a kinetic energy of (4026 ± 39) keV/u, which is in good agreement with the results of the phase probe measurement discussed above. A partially decelerated component with an energy of (2302 ± 96) keV/u is visible right below the undecelerated beam, and on the bottom of the screen, the completely decelerated ions can be observed with an energy of (489 ± 3) keV/u. This result agrees with preliminary observations in previous beamtimes [63] and is

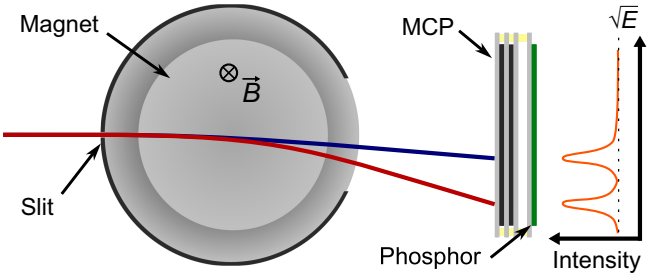

FIG. 5. One-shot energy analyzer for the separation of energy components. The incoming ion beam is deflected by a permanent magnet depending on its energy, and detected by an MCP detector with a phosphor screen.

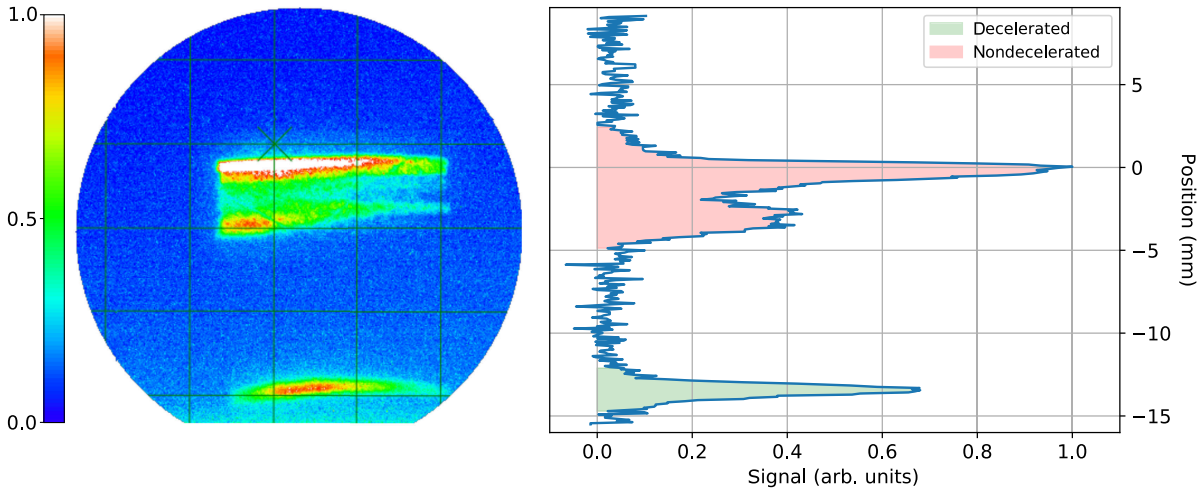

FIG. 6. Left: exemplary result from the one-shot energy analyzer following the IH structure. $^{36}Ar^{18+}$ ions are separated by the magnetic field, with the low-energy components located at the bottom and the high-energy components at the top. Right: intensity projected onto the vertical axis. The fully decelerated components are marked green and the partially or nondecelerated components are marked red.

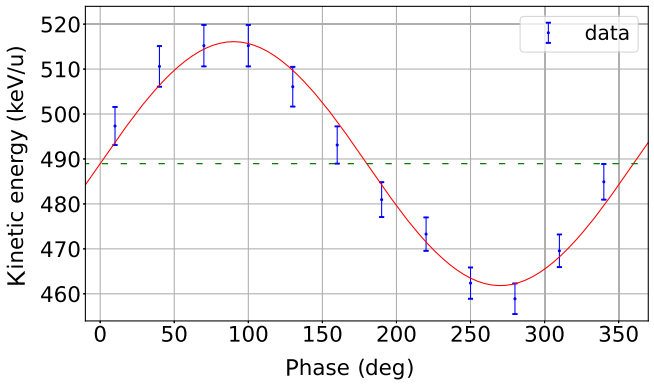

FIG. 7. Energy of the decelerated $^{36}Ar^{18+}$ ions as extracted from the one-shot energy analyzer over the phase setting of the rebuncher. A sine function (orange curve) is fitted to the data. The crossing points with the green dashed line correspond to no acceleration by the buncher, thereby indicating the ideal bunching conditions. The uncertainties of the data points are determined by how accurately the position of the decelerated ions on the energy analyzer could be determined. For this measurement, this is conservatively estimated to ± 0.1 mm, resulting in the presented uncertainties after conversion to energy values.

well inside the acceptance range of the RFQ, which is expected to be (485 ± 10) keV/u [51].

Before the ions are further decelerated in the RFQ, the shape of the microbunches is refined by the rebuncher, a third single buncher. When configured with the appropriate phase relative to the preceding cavities, this buncher serves to refine the shape of the bunches. In the case of a 180° mismatch, the buncher operates in the debunching mode, and for values in between, it can also slightly accelerate or decelerate the ions. As the buncher is located right before the energy analyzer, the phase settings for no change in kinetic energy can be determined by observing the position of the decelerated ion beam. This was already observed and employed in previous beamtimes at HITRAP [65].

The kinetic energy of the ions is plotted in Fig. 7 over the phase setting of the rebuncher. It is evident from the figure that a mismatch of the buncher's phase can result in an acceleration or deceleration of the ion beam by up to 30 keV/u. Fitting a sine function to the data yields phase values of 0° and 180° without any alteration in kinetic energy. However, it is not possible to assign these two zero crossings to bunch compression and expansion at this point, as this requires an analysis of the rebuncher in combination with the RFQ, taking into account the deceleration efficiency and phase acceptance of the RFQ. But observing the yield of decelerated ions after the RFQ provides a clear signature for optimizing the configuration of the rebuncher, as the highest deceleration efficiency and yield can only be achieved in bunching mode.

B. RFQ

With the optimized settings for the IH structure and the rebuncher, the decelerated beam can be guided through the cavity of the RFQ. As the high-energy ions remain in the beamline, it is again necessary to separate the beam into its energy components. This is achieved by means of a second permanent dipole magnet with a 100-mT field, which is located after the RFQ. The combination of this magnet with an MCP in the subsequent diagnostic chamber allows for the separation of the 4 MeV/u ions from the 0.5 MeV/u component. With the help of irises installed at the entrance and exit of the RFQ, the 0.5 MeV/u component is aligned along the central axis of the cavity.

At this point, the rf field of the RFQ is activated which further decelerates the ions to a final energy of 6–7 keV/u, provided the correct configuration of the rf phase and amplitude has been chosen. Thereafter, the ions are guided through the low-energy beamline that connects the RFQ with the Cooling Trap, where they are detected by an off-axis MCP detector located in the final diagnostic chamber before the trap. In order to separate the fully decelerated ions from those that are not or only partially decelerated, this detector is placed in parallel to the beamline axis. The slow ions are deflected onto the MCP detector by an electrostatic potential at a copper plate that is installed opposite to the MCP front plate. The applied 12 kV deflects the fully decelerated ions onto the MCP, while the partially or nondecelerated ions pass the detector nearly uninfluenced, thereby providing a background-free signal, a very similar scheme to the one that has been applied first by Daly in order to suppress neutral ions in a mass spectrometer [66].

This signal allows for a first characterization of the RFQ. In Fig. 8, the observed signal of decelerated ions is plotted over the phase (top) and the applied power (bottom) of the RFQ. The high uncertainties are attributed to substantial fluctuations in the observed signal in the order of ±25%. Within the limits of these uncertainties, a plateau is observed in the region between 70° and 90° with a rapid decline on either side. This roughly corresponds to the difference of the 20° phase width of the ion bunches extracted from the IH structure and the 45° phase acceptance of the RFQ [48]. Starting at a minimal power value of 32 kW, the deceleration efficiency in the RFQ steadily increases until a maximum is reached at 59 kW. From this point on, the observed signal remained constant for higher rf amplitudes, which is in good agreement with the initial commissioning measurement after construction of the cavity [51].

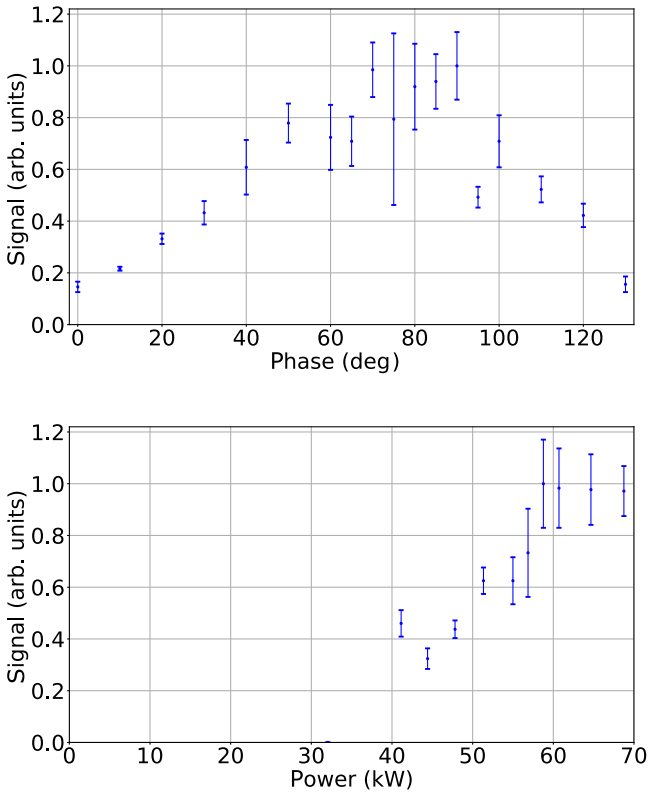

FIG. 8. Top: ion signal on the off-axis MCP detector after deceleration in the RFQ plotted over the rf phase at a power of 61 kW. Bottom: signal after deceleration in the RFQ plotted against the rf power at a phase of 89°. The ion species for both plots is $^{36}Ar^{18+}$ and the uncertainties represent the 1σ statistical uncertainty for each data point in both plots.

IV. FIRST RESULTS FROM THE COOLING TRAP

After the successful recommissioning and deeper characterization of the rf cavities, the last remaining step toward an operational HITRAP facility is the commissioning of the Cooling Trap. This process can be divided into two major milestones: the capture of accelerator-produced HCI and electron cooling of HCI in a Penning trap. The first of these milestones was achieved during the same commissioning beamtime discussed above with $^{36}Ar^{18+}$ and is presented in the following section. Because of the limited availability of accelerator beamtime, the second milestone could not yet be demonstrated with accelerator-produced ions. Instead, a local ion source was utilized to commission the Cooling Trap outside the beamtime periods. The results of this offline commission including the very first demonstration of electron cooling on highly charged ions in a Penning trap are presented in Sec. IV A.

A. Storage of accelerator-produced HCI

Following the deceleration by the two linear decelerators, the ions are guided to the Cooling Trap, the final preparation step at HITRAP. In this Penning trap, the ions will undergo electron cooling, thereby preparing them for subsequent experiments. The first step in this process is the capture of accelerator-produced ions. Coming from the RFQ, the ions have a kinetic energy of 6–7 keV/u, or 12–14 keV/q for $^{36}Ar^{18+}$ with a mass-to-charge ratio of 2. Moving from the velocity-dependent rf structures to the electrostatic Penning trap, from this point on the energy will be given in values per charge unit, as the operation of the trap is charge dependent.

To facilitate the ion capture process and allow for the required blocking potentials of more than 14 kV, the whole trap setup is biased by 9 kV with respect to ground. Applying additional 6 kV to the trap's outmost capture electrodes results in a total potential of 15 kV with respect to ground, sufficient to block and capture the incoming ion beam. For this, the ions are initially blocked at the far-side capture electrode, at which point the entrance-side capture electrode is also switched from 9 to 15 kV. The ions are

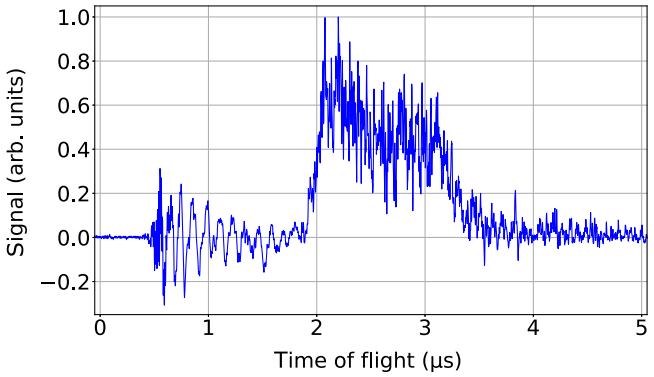

FIG. 9. Typical signal of accelerator-produced $^{36}Ar^{18+}$ ions after confinement and ejection from the Cooling Trap. In this particular case, the ions are stored for 100 ms, subsequently ejected, and then detected by an MCP detector.

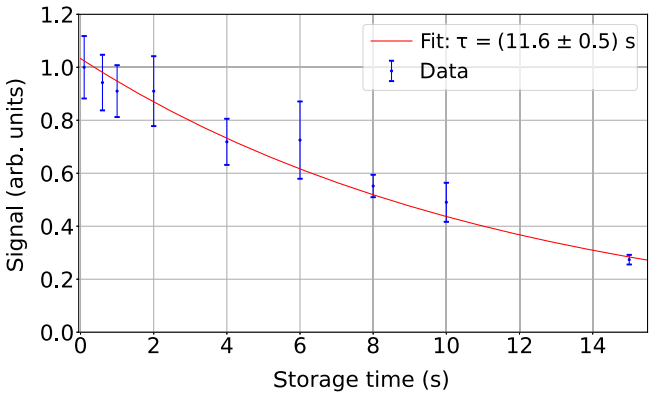

FIG. 10. Signal of confined and ejected ions from the Cooling Trap plotted over various storage times. The error bars of the data represent the 1σ statistical uncertainty. Fitting an exponential decay to the data yields a particle lifetime of (11.6 ± 0.5) s for the accelerator-produced $^{36}Ar^{18+}$ ions. We note that the uncertainty of the lifetime has been corrected for the small χ^2_{red} of the fit.

now confined within the Penning trap for a predefined storage time before the far-side capture electrode is lowered back to 9 kV, releasing the bunch of captured ions. The kinetic energy of the ejected ions can be set by adjusting the offset potential of the setup. To illustrate, lowering the potential during the storage from the initial 9 kV to ground will reduce the ions' kinetic energy after ejection by 9 keV$/q$, as compared to their energy after deceleration in the RFQ.

After ejection, the ions are picked up by an MCP detector producing the signal presented in Fig. 9. In this case, the storage time was set to 100 ms. The time axis is relative to the signal that triggers the switching of the capture potential, i.e., the ejection of the ions from the trap. Electrical noise, produced by the rapid switching of the capture potential, becomes visible at approximately 0.5 μs, before the ion signal starts at a time of flight of 1.9 μs, which is determined by the adjustable ions' kinetic energy after extraction from the trap. For future operation, the ion energy after extraction from the Cooling Trap will be 5 keV$/q$. With the higher mass-to-charge ratios of heavy isotopes such as uranium, the arrival time will shift toward higher values, resulting in an even better separation between electrical noise and ion-induced signal.

After the bunch length of (1.32 ± 0.04) μs, the signal rapidly drops to a level approaching that of background. The length of the bunch is predominantly determined by the velocity of the ions inside the trap and the trap's length. The first ions to arrive at the detector are those in close proximity to the ejection-side electrode and moving toward the detector when the trap is opened. Conversely, the last ions are at the same position but moving away from the detector, thus traversing the trap twice before exiting.

Extracting a precise number of ions captured and ejected is not possible with the employed MCP detector setup. However, a comparison of the signal with measurements performed with the local EBIT ion source provides an estimate of the order of 10^4 ejected ions. With increasing storage times, this number will decline as a result of various loss processes in the Cooling Trap. The most dominant process is anticipated to be charge exchange with residual gas, which is a crucial factor in the context of highly charged ions. Furthermore, elastic scattering and loss due to unstable ion trajectories cannot be disregarded. All these effects limit the lifetime of an ion in a Penning trap, which can be quantized by observing the ion signal for various storage times. The results of such a measurement series are presented in Fig. 10, where the ion signal is plotted over the storage time in the trap. For each data point, the ion signal of ten consecutive injections is averaged. The large error bars, which represent the 1σ statistical uncertainty for each data point, are a result of the strong shot-to-shot fluctuations. Fitting an exponential decay onto the data yields a lifetime of $\tau = (11.6 \pm 0.5)$ s, where τ denotes the time at which the signal intensity is reduced to $1/e$ of its original value at a storage time of 0 s. The resulting fitting parameters include a correction for χ^2_{red}.

It should be noted that an ion that undergoes charge exchange with residual gas may remain confined within the trap. It is only after the exchange of multiple electrons that the energy per charge of an ion will increase to a level where it can no longer be confined by the applied capture potentials. Consequently, the signal observed after ejection at the MCP detector may consist of multiple charge states that cannot be distinguished. For the purposes of subsequent experiments, however, an ion is already considered lost if it changes its charge state. Therefore, the charge state lifetime of the ion is shorter than the extracted value. The cause of this comparatively short lifetime is an unusually high pressure inside the Cooling Trap, a consequence of a vacuum leak in the setup. This leak was fixed after the beamtime, resulting in improved vacuum conditions and longer lifetimes, as demonstrated below in Sec. IV B.

In order to separate the target charge state from the ones created during storage and electron cooling, the vertical beamline starts with a 90° magnetic dipole accompanied with a slit system to reach the required resolution [67]. This step, which is planned for the next campaigns, will also enable the first investigation of charge exchange rates between heavy, highly charged ions and residual gas inside an ion trap. Because of the challenges associated with the production of heavy HCI at rest, HITRAP will provide unique possibilities in this regard. Already in the current state presented here, the facility is capable of providing large amounts of slow heavy HCI with a broad energy distribution. This enables experiments with negligible dependencies on the energy width, such as surface ionization studies [32]. Also, experiments that require only single ions are already feasible [5].

B. Electron cooling of HCI

After the successful storage of accelerator-produced ions, the last remaining step toward the completion of the HITRAP facility is the demonstration of electron cooling on highly charged ions. As the availability of HCI from the GSI accelerator is limited to short beamtime periods, the commissioning of electron cooling in the Penning trap is performed with ions from a local ion source. At HITRAP, a compact EBIT ion source can deliver intense pulses of the order of 10^5 highly charged ions at an arbitrary charge state up to Xe^{44+} [68,69]. This room-temperature Dresden EBIT is based on permanent magnets and was developed and manufactured by DREEBIT. It also provides ions for the commissioning of setups and even first experimental runs [70,71].

In order to achieve conditions comparable to those of heavy ions, such as hydrogenlike uranium with a mass-to-charge ratio of approximately 2.6, $^{40}Ar^{16+}$ with a ratio of 2.5 is selected for the commissioning phase. Following production by the EBIT, bunches containing approximately 10^5 ions are guided to the Cooling Trap at a kinetic energy of 4 keV/q, which corresponds to 1.6 keV/u for the given mass-to-charge ratio of 2.5. Typical beam parameters are summarized in Table I. The ions are then captured in-flight between the capture electrode by switching the applied potentials from ground to 7 kV.

Varying the storage time and detecting the ions after ejection on an MCP detector allows again for the determination of their lifetime in the trap, as previously described for accelerator-produced ions. The result of this measurement series is shown in Fig. 11, where the detected signal is plotted against the storage time in the trap. Fitting an exponential decay onto the data yields in this case a lifetime of (72.8 ± 3.2) s, which is considerably longer than for accelerator-produced $^{36}Ar^{18+}$ due to better vacuum conditions compared to those during the beamtime.

TABLE I. Typical beam parameter for ions arriving at the Cooling Trap from the RFQ and EBIT. The emittance values are extracted from simulations [53,68].

	Mean energy	Energy width	Emittance
RFQ	6.5 keV/u	1 keV/u	100π mm mrad
EBIT	4 keV/q	< 5 eV/q	20π mm mrad

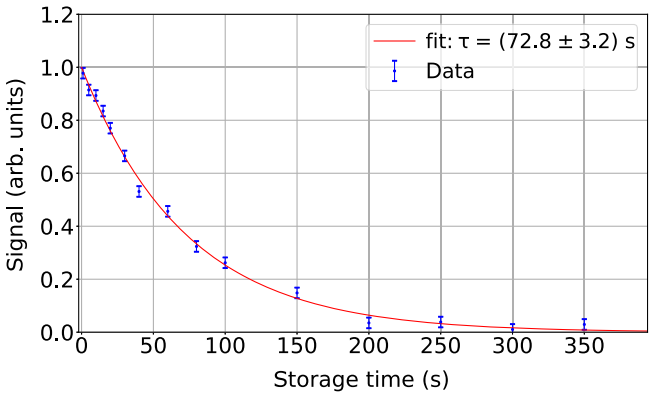

FIG. 11. Signal of captured and ejected $^{40}Ar^{16+}$ ions from the EBIT detected on an MCP detector plotted over various storage times in the Cooling Trap. The 1σ statistical uncertainty is represented by the error bars of the data points. Fitting an exponential decay to the data results in a particle lifetime of (72.8 ± 3.2) s.

Electron cooling requires the simultaneous storage of ions along with the electron plasma in a nested-trap configuration, as discussed in Sec. II B. First, the electrons are captured between the two long end cap electrodes. The number of stored electrons can now be increased by stacking multiple injections in a positive potential applied to the central ring electrode, which in turn also increases the plasma density. Following the plasma preparation stage, the ions are injected and captured between the two outmost capture electrodes. Ions and electrons are now confined within overlapping volumes, enabling the transfer of kinetic energy from the ions to the electrons. After a predetermined time of simultaneous storage, the ions are ejected toward the off-axis MCP detector in the low-energy beamline.

The detected signal for 2 s of storage with stacking ten consecutive injections of electrons is plotted in Fig. 12 in red against the ions' time of flight to the detector. As a reference, the signal without cotrapped electrons is also shown in blue. The trapping schemes and applied potentials for both datasets are identical, with the sole exception of the electron production which is omitted for the reference measurement. The detected ion signal of the measurement with electrons commences a few hundred nanoseconds later compared to the reference measurement without a cotrapped electron plasma. Taking the initial kinetic energy of the ions and the difference in time of flight into account, in the given example the ions' energy is reduced from 4 to

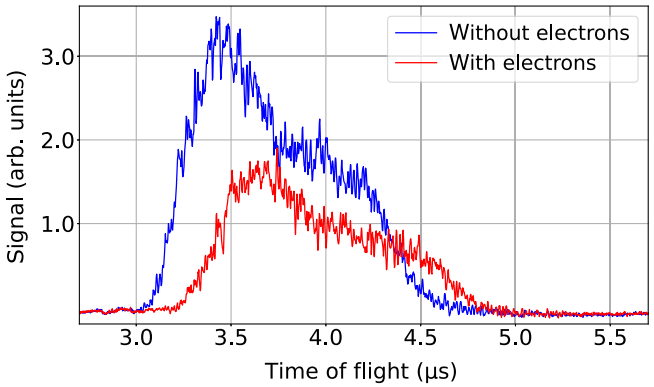

FIG. 12. Signal of EBIT-produced $^{40}Ar^{16+}$ ions stored for 2 s simultaneously with an electron plasma plotted in red over the ions' time of flight to the MCP detector. For reference, the ion signal in absence of a cotrapped electron plasma is plotted in blue. The difference in time of flight indicates an energy transfer from the ions to the electron plasma.

(3.6 ± 0.1) keV$/q$, which proves the transfer of energy from the highly charged ions to the electron plasma. It should be noted that the shape of the signal is not an indicator of the ions' energy distribution. Instead, it is determined completely by the geometrical length of the trap and the kinetic energy of the ions. The first detected ions are those closest to the exit and moving toward the detector when opening the trap, while the last ions are moving away and traverse the trap once more. Furthermore, ions in proximity to the turning point at the capture electrodes have less kinetic energy in comparison to those in the trap center. When a capture electrode is opened during the ejection process, these ions move slower toward the detector, resulting in the asymmetric shape of the signal.

In addition to the increased time of flight to the detector, also a reduction in signal intensity is observed. This is not attributed to an increased rate of ion loss, but rather to a decrease in transport efficiency toward the detector due to changing optics parameters for different beam energies. However, it was observed that the application of a positive offset potential to the entire setup during the storage period can be employed to accelerate the ions upon extraction, which compensates the reduction of the mean kinetic energy and restores the original signal intensity.

The kinetic energy after simultaneous storage calculated from the difference in time of flight does not take into account any charge exchange of the ions with residual gas or recombination with the electron plasma. To gain further insight into this matter, it is necessary to separate the charge states after ejection. Therefore, another set of measurements was performed after a retarding field energy analyzer was installed at HITRAP, which is schematically depicted in Fig. 13. This approach relies on the assumption that the total kinetic energy of an ion remains constant during a change in its charge state. Consequently, the ions differ in their kinetic energy per charge, and can be separated by a

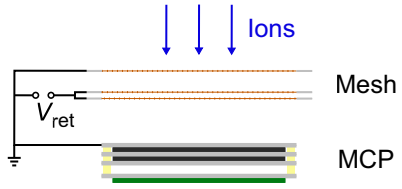

FIG. 13. Schematic layout of the retarding field energy analyzer. The second and third meshes from the top are biased by a retarding field potential, denoted here as V_{ret}. It is only the ions with sufficient kinetic energy per charge that are able to overcome the potential and thereby contribute to the signal observed on the MCP detector.

retarding electric field. The signal intensity is measured with the MCP detector while the potential applied to the mesh is increased stepwise, thus allowing for extracting the energy-per-charge distribution of the ion bunch. Assuming that the charge states are indeed clearly separated in the energy-per-charge domain, a step function is expected when plotting the ion signal of the retarding field. Each step in the signal should thus represent the energy distribution of a specific charge state.

To improve the transport efficiency toward the detector, the potential of the trap setup is increased during the storage time to accelerate the ion upon extraction. This bias potential V_{trap} is chosen such that the ions are accelerated approximately to the optimal transport energy of 4 keV$/q$. As all ions, independent of their charge state, gain the same energy per charge, the kinetic energy per charge of the stored ions can be simply derived by subtracting a constant value from the measured value. The kinetic energy per charge of the trapped ions E_{kin}/q is then given by

$$E_{kin}/q = e(V_{ret} - V_{trap}), \tag{5}$$

with the elementary charge e and the retarding field potential V_{ret}.

The results of this measurement series are presented in Fig. 14, where the ion signal is plotted over the applied retarding field potential minus the bias potential $V_{ret} - V_{trap}$. The blue data points are obtained in measurements without electron injection, whereas the red ones are taken with cotrapped electrons. Although the expected stepwise decrease is not observed, this does not allow us to conclude that the beam contains only a single charge state, as the following analysis will demonstrate: The data can be described by the distribution

$$f(V_{ret}) = \int_{V_{ret}}^{\infty} f(E_{\parallel}) \mathrm{d}E_{\parallel}, \tag{6}$$

with $f(E_{\parallel})$ being the longitudinal kinetic energy distribution. Only ions with an energy per charge in the velocity component parallel to the electric field $E_{\parallel}$ that exceeds the

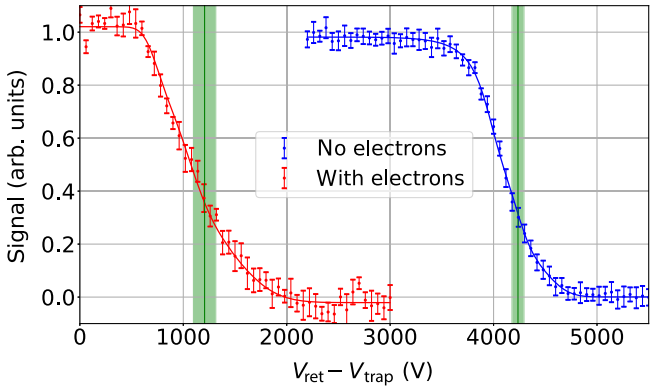

FIG. 14. Red: measured signal of EBIT-produced $^{40}Ar^{16+}$ ions at the retarding field energy analyzer after 2 s of simultaneous storage with an electron plasma plotted over the applied retarding field potential. The data are fitted with Eq. (6) which yields a central kinetic energy of (1.21 ± 0.11) keV$/q$ as indicated by the green bar. As a reference, the same measurement was performed with no cotrapped electrons resulting in the blue dataset. In this case, the fit yields a central energy of (4.24 ± 0.06) keV$/q$. The 1σ statistical uncertainty is for both plots represented by the error bars of each data point.

applied potential can pass. Consequently, the observed signal shape depends on both the distribution of the total kinetic energy E and the distribution of the angle θ under which the ions pass the mesh, as described by the relation

$$E_{\parallel} = E\cos^2(\theta). \tag{7}$$

The detector measures all ions with a combination of total kinetic energy and impact angle that allows them to pass the retarding field. Assuming Gaussian-shaped distributions of total energy and angle with central values of E_0 and θ_0 and standard deviations σ_E and σ_θ, respectively, integrating the joint distribution of energy and angle over all possible angles defines the distribution of the kinetic energy in the longitudinal component as

$$f(E_{\parallel}) = \frac{A}{2\pi\sigma_E\sigma_\theta} \times \int_{-\pi/2}^{\pi/2} \exp\left(-\frac{\left(\frac{E_{\parallel}}{\cos^2(\theta)} - E_0\right)^2}{2\sigma_E^2} - \frac{(\theta-\theta_0)^2}{2\sigma_\theta^2}\right) \mathrm{d}\theta. \tag{8}$$

The parameter A represents here the amplitude of the distribution.

Fitting Eq. (6) to the data allows for the extraction of the central kinetic energy, as indicated in Fig. 14 by the green bar. The width of the green bar represents here the uncertainty of the extracted mean kinetic energy, not the width of the energy distribution. As the signal declines continuously with increasing retarding fields, the charge states are not clearly distinguishable. This can be attributed to the angle distribution of the ions hitting the detector. The detector cannot distinguish between low-energy ions arriving perpendicular to the meshes and ions with higher energy entering the retarding field under a different angle. This widens the detected energy distribution of a single charge state so far that it overlaps with the neighboring states, resulting in the observed continuous decrease. During the analysis, the data were fitted assuming various amounts of different charge states in the observed signal. The best description of the data is achieved with the assumption of three present charge states, namely, 16+, 15+, and 14+, as it is presented here.

The indistinguishable charge states also lead to a strong correlation between the fit parameters, thereby limiting the gained information to the central energy of the whole distribution. For the red dataset in Fig. 14, ions are stored for 2 s with an electron plasma comprising 40 consecutive injections and accelerated by a bias potential of 3 kV which yields a central energy of (1.21 ± 0.11) keV$/q$ during the storage. As a reference, the measurement is performed without cotrapped electrons and no postacceleration, as represented by the blue dataset in Fig. 14. The central energy of solely stored ions is here (4.24 ± 0.06) keV$/q$. This value is higher than the 4 keV$/q$ of the injected ions, as the energy per charge increases during charge exchange with residual gas while the total energy remains constant. The results demonstrate a clear transfer of kinetic energy and show the applicability of electron cooling on highly charged ions in a Penning trap and, consequently, the feasibility of providing high intensity bunches of accelerator-produced HCI.

The next step of HITRAP will be the charge state analysis by passing through a magnetic bender to properly account for charge exchange and recombination during the cooling process. This will allow for a more detailed investigation of electron cooling, also with respect to cooling the energy distribution.

V. SUMMARY

Following an eight-year period of shutdown, the commissioning process of the HITRAP facility was resumed in 2022, with the successful deceleration of $^{58}Ni^{28+}$ from 4 MeV/u down to approximately 6 keV/u. This step was routinely repeated in the following beamtimes also with other ion species. This allowed for the first two experimental campaigns at HITRAP that investigated the interaction between decelerated bare gold ions Au^{79+} at 6 keV/u with 2D surfaces.

In addition, decelerated $^{36}Ar^{18+}$ ions were for the first time captured in the Cooling Trap, to date a unique achievement. The observed lifetime of (11.6 ± 0.5) s is adequate for the application of electron cooling and pending further improvement. Following their storage in

the Penning trap of up to 15 s, the ions were ejected at a selected kinetic energy and detected in the adjacent beamline.

Between beamtimes with accelerator-produced ions, the Cooling Trap was commissioned with $^{40}Ar^{16+}$ ions from the local EBIT ion source. Bunches of approximately 10^5 ions were captured in the Penning trap, with an observed lifetime of (72.8 ± 3.2) s. Furthermore, it has been demonstrated that more than 10^9 electrons, provided by a pulsed photoionization source, can be captured with a single injection. The number of confined electrons can be further increased by stacking multiple injections in the trap, allowing for higher plasma densities. The stored electrons were also employed to improve the alignment of the magnetic and electric fields through the observation of their magnetron motion. This, in turn, led to significantly higher plasma densities and also enhanced the spatial overlap between simultaneously stored electrons and ions. These improvements ultimately culminated in the worldwide first observation of electron cooling of highly charged ions in a Penning trap. During short cooling periods of only 2 s, the mean kinetic energy of the ions could be reduced to a selected value below the initial 4 keV$/q$.

Together with the successful deceleration and storage of accelerator-produced ions, the HITRAP facility offers unique opportunities in heavy-ion research, as experiments requiring single ions at rest or large amounts of slow ions with a broad energy distribution are already feasible.

VI. OUTLOOK

The next two milestones of the HITRAP facility are the demonstration of the reduction of the energy width through electron cooling and its application also to accelerator-produced heavier HCI. The first milestone necessitates the clear separation of charge states subsequent to the ejection of the ions from the Cooling Trap. This step will require certain changes in the injection beamline, as the same segment is to be used quasisimultaneously for counter-propagating ion beams during the commissioning with ions from the EBIT.

Most recently, the HITRAP decelerator was tested with $^{107}Ag^{45+}$ ions from the GSI accelerator in February 2025. The ions were successfully decelerated and trapped simultaneously with electrons, when an interaction between the ions and electrons could be observed, but no clear sign of electron cooling was evident. A detailed analysis is currently underway. The now routinely achieved deceleration in the IH structure and the RFQ also allowed for the first two experimental campaigns at the HITRAP facility in March 2025. During this beamtime with aim of studying the interaction between heavy HCI and 2D surfaces, bare gold nuclei could be decelerated to approximately 6 keV/u and were guided onto several targets. To date, the necessary quantities of heavy HCI for these kinds of experiments are only available at the HITRAP facility, thereby offering unparalleled opportunities for the study of slow heavy HCI. In the forthcoming beamtimes, the primary objective will be to store accelerator-produced HCI simultaneously with an electron plasma and to provide definitive evidence of electron cooling, both through the reduction of the mean kinetic energy and the energy width. This will then also enable the efficient transport along the beamline and through the deflection magnet, in turn allowing for an investigation of the effect of electron cooling on the width of the ions' energy distribution as well as the charge exchange and recombination rates in the Penning trap.

When running at full scope, the HITRAP facility will provide even more possibilities in the heavy-ion research, allowing for high precision experiments on slow ions or ions at rest. As the facility is capable of decelerating any ion species with m/q ratios smaller than 2.7, available ions will range from protons to bare uranium. While the light and medium-heavy ions will be produced in local EBIT ion sources [58,72], the heavier side of this range will be produced by the GSI accelerators and subsequently decelerated at HITRAP. The foreseen maximal intensity of heavy highly charged ions delivered by the HITRAP facility amounts to 10^6 ions per bunch, limited only by the amount of ions stored in the ESR and the deceleration efficiency at HITRAP. While the lightest ions can be produced in an EBIT at a rate of several bunches per second, for the heaviest ions about one bunch per minute can be expected. The transport energy will be in the order of 5 keV$/q$ with a width of 10 eV after electron cooling. At present, several experimental setups are already in various commissioning stages at HITRAP, ranging from testing QED in extreme fields [29,42,73] to surface interaction studies [32] and new frequency standards with heavy HCI [5].

ACKNOWLEDGMENTS

We acknowledge financial support from the German Federal Ministry for Research, Technology and Space under Grants No. 05P21RDFA1 and No. 05P24RD5.

DATA AVAILABILITY

The datasets generated in the experiment and analyzed for the current study are publicly available at [74].

[1] J. B. Greenwood, R. J. Mawhorter, I. Čadež, J. Lozano, S. J. Smith, and A. Chutjian, *The contribution of charge exchange to extreme ultra-violet and X-ray astronomy*, Phys. Scr. **2004**, 358 (2004).

[2] S. Pilling, E. Seperuelo Duarte, E. F. da Silveira, E. Balanzat, H. Rothard, A. Domaracka, and P. Boduch, *Radiolysis of ammonia-containing ices by energetic, heavy,*

and highly charged ions inside dense astrophysical environments, Astron. Astrophys. **509**, A87 (2010).

[3] N. Hell, P. Beiersdorfer, G. V. Brown, M. E. Eckart, R. L. Kelley, C. A. Kilbourne, M. A. Leutenegger, T. E. Lockard, F. S. Porter, and J. Wilms, *Highly charged ions in a new era of high resolution X-ray astrophysics*, X-Ray Spectrom. **49**, 218 (2020).

[4] S. A. King, L. J. Spieß, P. Micke, A. Wilzewski, T. Leopold, E. Benkler, R. Lange, N. Huntemann, A. Surzhykov, V. A. Yerokhin *et al.*, *An optical atomic clock based on a highly charged ion*, Nature (London) **611**, 43 (2022).

[5] P. Micke, T. Leopold, S. King, E. Benkler, L. Spieß, L. Schmoeger, M. Schwarz, J. Crespo López-Urrutia, and P. Schmidt, *Coherent laser spectroscopy of highly charged ions using quantum logic*, Nature (London) **578**, 60 (2020).

[6] M. S. Safronova, V. A. Dzuba, V. V. Flambaum, U. I. Safronova, S. G. Porsev, and M. G. Kozlov, *Highly charged ions for atomic clocks, quantum information, and search for α variation*, Phys. Rev. Lett. **113**, 030801 (2014).

[7] A. V. Volotka, D. A. Glazov, G. Plunien, and V. M. Shabaev, *Progress in quantum electrodynamics theory of highly charged ions*, Ann. Phys. (Amsterdam) **525**, 636 (2013).

[8] V. M. Shabaev, D. A. Glazov, M. B. Shabaeva, V. A. Yerokhin, G. Plunien, and G. Soff, *g factor of high-Z lithiumlike ions*, Phys. Rev. A **65**, 062104 (2002).

[9] V. M. Shabaev, *Hyperfine structure of hydrogen-like ions*, J. Phys. B **27**, 5825 (1994).

[10] X. Fan, T. G. Myers, B. A. D. Sukra, and G. Gabrielse, *Measurement of the electron magnetic moment*, Phys. Rev. Lett. **130**, 071801 (2023).

[11] H. Häffner, T. Beier, N. Hermanspahn, H.-J. Kluge, W. Quint, S. Stahl, J. Verdú, and G. Werth, *High-accuracy measurement of the magnetic moment anomaly of the electron bound in hydrogenlike carbon*, Phys. Rev. Lett. **85**, 5308 (2000).

[12] S. Sturm, A. Wagner, B. Schabinger, J. Zatorski, Z. Harman, W. Quint, G. Werth, C. H. Keitel, and K. Blaum, *g factor of hydrogenlike* $^{28}Si^{13+}$, Phys. Rev. Lett. **107**, 023002 (2011).

[13] J. Verdú, S. Djekić, H. Haffner, S. Stahl, T. Valenzuela, M. Vogel, G. Werth, T. Beier, H.-J. Kluge, and W. Quint, *Electronic g factor of hydrogenlike oxygen* $^{16}O^{7+}$, Phys. Rev. Lett. **92**, 093002 (2004).

[14] Sven Sturm, Manuel Vogel, Florian Köhler-Langes, Wolfgang Quint, Klaus Blaum, and Günter Werth, *High-precision measurements of the bound electron's magnetic moment*, Atoms **5**, 4 (2017).

[15] J. Morgner, B. Tu, C. König, T. Sailer, F. Heiße, H. Bekker, B. Sikora, C. Lyu, V. Yerokhin, Z. Harman *et al.*, *Stringent test of QED with hydrogen-like tin*, Nature (London) **622**, 53 (2023).

[16] S. Sturm, G. Werth, and K. Blaum, *Electron g-factor determinations in Penning traps*, Ann. Phys. (Amsterdam) **525**, 620 (2013).

[17] N. P. M. Brantjes, *The g-factor of hydrogen-like heavy ions as a test for QED*, Ph.D. thesis, Ruperto-Carola Universität, Heidelberg, 2012.

[18] T. Sailer, V. Debierre, Z. Harman, F. Heiße, C. König, J. Morgner, B. Tu, A. V. Volotka, C. H. Keitel, K. Blaum *et al.*, *Measurement of the bound-electron g-factor difference in coupled ions*, Nature (London) **606**, 479 (2022).

[19] J. Schwinger, *On gauge invariance and vacuum polarization*, Phys. Rev. **82**, 664 (1951).

[20] T. Beier, *The* g_j *factor of a bound electron and the hyperfine structure splitting in hydrogenlike ions*, Phys. Rep. **339**, 79 (2000).

[21] V. Hannen *et al.*, *Lifetimes and g-factors of the HFS states in H-like and Li-like bismuth*, J. Phys. B **52**, 085003 (2019).

[22] D. L. Moskovkin, N. S. Oreshkina, V. M. Shabaev, T. Beier, G. Plunien, W. Quint, and G. Soff, *g factor of hydrogenlike ions with nonzero nuclear spin*, Phys. Rev. A **70**, 032105 (2004).

[23] V. M. Shabaev, D. A. Glazov, G. Plunien, and A. V. Volotka, *Theory of bound-electron g factor in highly charged ions*, J. Phys. Chem. Ref. Data **44**, 031205 (2015).

[24] V. M. Shabaev, A. N. Artemyev, V. A. Yerokhin, O. M. Zherebtsov, and G. Soff, *Towards a test of QED in investigations of the hyperfine splitting in heavy ions*, Phys. Rev. Lett. **86**, 3959 (2001).

[25] I. Klaft, S. Borneis, T. Engel, B. Fricke, R. Grieser, G. Huber, T. Kühl, D. Marx, R. Neumann, S. Schröder, P. Seelig, and L. Völker, *Precision laser spectroscopy of the ground state hyperfine splitting of hydrogenlike* $^{209}Bi^{82+}$, Phys. Rev. Lett. **73**, 2425 (1994).

[26] M. Horst, Z. Andelkovic, C. Brandau, R. J. Chen, D. Freire Fernández, C. Geppert, J. Glorius, V. Hannen, R. Heß, P. Imgram *et al.*, *Storage-ring laser spectroscopy of accelerator-produced hydrogen-like* $^{208}Bi^{82+}$, Nat. Phys. **21**, 1057 (2025).

[27] J. Ullmann, Z. Andelkovic, C. Brandau, A. Dax, W. Geithner, C. Geppert, C. Gorges, M. Hammen, V. Hannen, S. Kaufmann *et al.*, *High precision hyperfine measurements in Bismuth challenge bound-state strong-field QED*, Nat. Commun. **8**, 15484 (2017).

[28] H.-J. Kluge *et al.*, *HITRAP: A facility at GSI for highly charged ions*, in *Current Trends in Atomic Physics*, Advances in Quantum Chemistry Vol. 53, edited by S. Salomonson and E. Lindroth (Academic Press, Amsterdam, 2008), pp. 83–98.

[29] Z. Andelkovic, R. Cazan, W. Nörtershäuser, S. Bharadia, D. M. Segal, R. C. Thompson, R. Jöhren, J. Vollbrecht, V. Hannen, and M. Vogel, *Laser cooling of externally produced Mg ions in a Penning trap for sympathetic cooling of highly charged ions*, Phys. Rev. A **87**, 033423 (2013).

[30] D. von Lindenfels, M. Wiesel, D. A. Glazov, A. V. Volotka, M. M. Sokolov, V. M. Shabaev, G. Plunien, W. Quint, G. Birkl, A. Martin, and M. Vogel, *Experimental access to higher-order Zeeman effects by precision spectroscopy of highly charged ions in a Penning trap*, Phys. Rev. A **87**, 023412 (2013).

[31] M. Vogel, Z. Andelkovic, G. Birkl, S. Ebrahimi, V. Hannen, D. v. Lindenfels, A. Martin, T. Murböck, W. Nörtershäuser, W. Quint, S. Schmidt, D. M. Segal, R. C. Thompson, J. Vollbrecht, W. Ch, and M. Wiesel, *Penning-trap experiments for spectroscopy of highly-charged ions at HITRAP*, Phys. Scr. **2015**, 014066 (2015).

[32] A. Niggas, M. Werl, F. Aumayr, and R. A. Wilhelm, *Charge exchange of slow highly charged ions from an electron beam ion trap with surfaces and 2D Materials*, J. Phys. B **57**, 072001 (2024).

[33] H. Winter and F. Aumayr, *Hollow atoms*, J. Phys. B **32**, R39 (1999).
[34] V. Shabaev, A. Bondarev, D. Glazov, Y. Kozhedub, I. Maltsev, A. Malyshev, R. Popov, D. Tumakov, and I. Tupitsyn, *QED with heavy ions: On the way from strong to supercritical fields*, in *Proceedings of the International Conference on Precision Physics and Fundamental Physical Constants—PoS(FFK2019)*, p. FFK2019 (Sissa Medialab, Trieste, 2019), p. 052.
[35] G. Zschornacka, M. Schmidt, and A. Thorn, *Electron beam ion sources*, arXiv:1410.8014.
[36] R. Becker, *Electron beam ion sources and traps*, Rev. Sci. Instrum. **71**, 816 (2000).
[37] N. D. Guise, S. M. Brewer, and J. N. Tan, *Highly charged ions in rare earth permanent magnet Penning traps*, in *New Trends in Atomic and Molecular Physics* (Springer, Berlin, 2013), Vol. 76.
[38] C. Schweiger, C. M. König, J. R. Crespo López-Urrutia, M. Door, H. Dorrer, C. E. Düllmann, S. Eliseev, P. Filianin, W. Huang, K. Kromer, P. Micke, M. Müller, D. Renisch, A. Rischka, R. X. Schüssler, and K. Blaum, *Production of highly charged ions of rare species by laser-induced desorption inside an electron beam ion trap*, Rev. Sci. Instrum. **90**, 123201 (2019).
[39] A. Girard, D. Hitz, G. Melin, and K. Serebrennikov, *Electron cyclotron resonance plasmas and electron cyclotron resonance ion sources: Physics and technology*, Rev. Sci. Instrum. **75**, 1381 (2004).
[40] Z. Q. Xie, *Production of highly charged ion beams from electron cyclotron resonance ion sources*, Rev. Sci. Instrum. **69**, 625 (1998).
[41] S. Creutzburg, A. Niggas, D. Weichselbaum, P. L. Grande, F. Aumayr, and R. A. Wilhelm, *Angle-dependent charge exchange and energy loss of slow highly charged ions in freestanding graphene*, Phys. Rev. A **104**, 042806 (2021).
[42] T. Murböck, S. Albrecht, Z. Andelkovic, R. Cazan, V. Hannen, R. Jöhren, J. Vollbrecht, S. Schmidt, D. Segal, R. Thompson, M. Vogel, C. Weinheimer, W. Nörtershäuser, and G. Birkl, *SpecTrap: Precision spectroscopy of highly charged ions—Status and prospects*, Phys. Scr. **2013**, 014096 (2013).
[43] R. E. Marrs, S. R. Elliott, and D. A. Knapp, *Production and trapping of hydrogenlike and bare uranium ions in an electron beam ion trap*, Phys. Rev. Lett. **72**, 4082 (1994).
[44] V. Shevelko, N. Winckler, and I. Y. Tolstikhina, *Stripping of relativistic uranium-ion beams by foils*, Nucl. Instrum. Methods Phys. Res., Sect. B **479**, 23 (2020).
[45] M. Steck and Y. A. Litvinov, *Heavy-ion storage rings and their use in precision experiments with highly charged ions*, Prog. Part. Nucl. Phys. **115**, 103811 (2020).
[46] Z. Andelkovic, S. Fedotova, W. Geithner, P. Gerhard, F. Herfurth, I. Kraus, M. Maier, A. Reiter, N. Stallkamp, and G. Vorobyev, *Preparation of low-energy heavy ion beams in a compact linear accelerator/decelerator*, in *Proceedings of the 15th International Conference on Heavy Ion Accelerator Technology (HIAT'22)* (JACoW Publishing, Geneva, Switzerland, 2022).
[47] B. Franzke, *The heavy ion storage and cooler ring project ESR at GSI*, Nucl. Instrum. Methods Phys. Res., Sect. B **24–25**, 18 (1987).
[48] L. Dahl, W. Barth, M. Kaiser, O. Kester, H. Kluge, W. Vinzenz, B. Hofmann, U. Ratzinger, A. Sauer, and A. Schempp, *The HITRAP decelerator project at GSI*, in *Proceedings of the EPAC 2006 Conference, Edinburgh, UK* (JACoW, Geneva, 2006), pp. 1568–1570.
[49] W. T. Milner, *Double-drift beam bunching systems*, IEEE Trans. Nucl. Sci. **26**, 1445 (1979).
[50] C. Kitegi, U. Ratzinger, and S. Minaev, *The IH cavity for HITRAP*, in *Proceedings of LINAC 2004, Lübeck, Germany* (JACoW, Geneva, 2004), pp. 54–56.
[51] M. Maier, K. Dermati, F. Herfurth, E. Kammer, M. König, N. Kotovskiy, M. Müller, D. Neidherr, R. Repnow, E. Scheurich, M. Trebis, H. Vormann, G. Vorobjev, P. Werle, and S. Yaramyshev, *Offline commissioning of the old and new HITRAP RFQ*, GSI Sci. Rep. 272 (2012), https://repository.gsi.de/record/52167/?ln=de.
[52] S. Yaramyshev, W. Barth, G. Clemente, L. Dahl, V. Gettmann, F. Herfurth, M. Kaiser, M. Maier, D. Neidherr, A. Orzhekhovskaya *et al.*, *A new design of the RFQ channel for GSI HITRAP facility*, in *Proceedings of the Linear Accelerator Conference LINAC2012, Tel-Aviv, Israel* (JACoW, Geneva, 2012).
[53] F. Herfurth, T. Beier, L. Dahl, S. Eliseev, S. Heinz, O. Kester, H. Kluge, C. Kozhuharov, G. Maero, W. Quint, and H. Collaboration, *Highly charged ions at rest: The HITRAP project at GSI*, AIP Conf. Proc. **793**, 278 (2005).
[54] F. Herfurth *et al.* (The HITRAP Collaboration), *The HITRAP facility for slow highly charged ions*, Phys. Scr. **2015**, 014065 (2015).
[55] G. Gabrielse, X. Fei, L. A. Orozco, R. L. Tjoelker, J. Haas, H. Kalinowsky, T. A. Trainor, and W. Kells, *Cooling and slowing of trapped antiprotons below 100 meV*, Phys. Rev. Lett. **63**, 1360 (1989).
[56] D. S. Hall and G. Gabrielse, *Electron cooling of protons in a nested penning trap*, Phys. Rev. Lett. **77**, 1962 (1996).
[57] S. F. Paul, *Precision mass measurements for the astrophysical rp-process and electron cooling of trapped ions*, Ph.D. thesis, Ruperto-Carola Universität, Heidelberg, 2023.
[58] Z. Andelkovic, J. Fischer, F. Herfurth, K. König, D. Neidherr, W. Nörtershäuser, M. Shroff, S. Trotsenko, and G. Vorobjev, *Development of the HITRAP Cooling Trap and the EBIT offline ion source*, Hyperfine Interact. **240**, 1 (2019).
[59] G. Maero, *Cooling of highly charged ions in a Penning trap for HITRAP*, Ph.D. thesis, Ruperto-Carola Universität, Heidelberg, 2008.
[60] G. Maero, F. Herfurth, O. Kester, H. Kluge, S. Koszudowski, and W. Quint, *Simulation of cooling mechanisms of highly-charged ions in the HITRAP cooler trap*, in *Proceedings of COOL 2007, Bad Kreuznach, Germany* (JACoW, Geneva, 2007), pp. 130–133.
[61] C. Krantz, *Intense electron beams from GaAs photocathodes as a tool for molecular and atomic physics*, Ph.D. thesis, Ruperto-Carola Universität, Heidelberg, 2009.
[62] J. Aoki, Y. Kiwamoto, Y. Soga, and A. Sanpei, *Novel application of electron vortex dynamics to the alignment of magnetic and cylinder axes*, Jpn. J. Appl. Phys. **43**, 7777 (2004).
[63] G. Vorobjev, C. Andre, W. Barth, E. Berdermann, G. Clemente, M. I. Ciobanu, L. Dahl, P. Forck, P. Gerhard,

R. Haseitl *et al.*, *Diagnostic scheme for the HITRAP decelerator*, in *Proceedings of the 10th European Workshop on Beam Diagnostics and Instrumentation for Particle Accelerators DIPAC2011, Hamburg, Germany* (JACoW, Geneva, 2015), pp. 311–313.

[64] F. Herfurth, W. Barth, G. Clemente, L. Dahl, P. Gerhard, M. Kaiser, O. Kester, H. Kluge, S. Koszudowski, C. Kozhuharov *et al.*, *HITRAP—Heavy, highly-charged ions and antiprotons at rest*, Acta Phys. Pol. B **41**, 457 (2010), https://www.actaphys.uj.edu.pl/index_n.php?I=R&V=41&N=2.

[65] F. Herfurth, Z. Andjelkovic, N. Brantjes, W. Barth, G. Clemente, L. Dahl, S. Fedotova, P. Gerhard, M. Kaiser, O. Kester *et al.*, *The HITRAP decelerator and beam instrumentation*, in *Proceedings of HIAT 2012, Chicago, IL, USA* (JACoW, Geneva, 2012), pp. 217–221.

[66] N. R. Daly, *Scintillation type mass spectrometer ion detector*, Rev. Sci. Instrum. **31**, 264 (1960).

[67] Z. Andelkovic, F. Herfurth, N. Kotovskiy, K. König, B. Maaß, T. Murböck, D. Neidherr, S. Schmidt, J. Steinmann, M. Vogel, and G. Vorobjev, *Beamline for low-energy transport of highly charged ions at HITRAP*, Nucl. Instrum. Methods Phys. Res., Sect. A **795**, 109 (2015).

[68] A. Sokolov, F. Herfurth, O. Kester, T. Stoehlker, A. Thorn, G. Vorobjev, and G. Zschornack, *SPARC EBIT—A charge breeder for the HITRAP project*, J. Instrum. **5**, C11001 (2010).

[69] B. O'Rourke, S. Geyer, A. Silze, A. Solokov, G. Vorobjev, D. Winters, O. Kester, and T. Stöhlker, *The SPARC EBIT at GSI: Commissioning and future plans at the HITRAP beamline*, J. Phys. Conf. Ser. **163**, 012103 (2009).

[70] K. Mohr, A. Buß, Z. Andelkovic, V. Hannen, M. Horst, P. Imgram, K. König, B. Maaß, W. Nörtershäuser, S. Rausch, R. Sánchez, and C. Weinheimer, *Collinear laser spectroscopy of helium-like* $^{11}B^{3+}$, Atoms **11**, 11 (2023).

[71] K. Kanika, *Studies and cooling of highly charged ion ensembles in the ARTEMIS trap and high-precision mass measurements of* ^{221}Fr, ^{219}Rn, ^{213}Bi, ^{211}Pb, ^{209}Pb, ^{207}Tl *and* ^{207}Pb *at SHIPTRAP*, Ph.D. thesis, Ruperto-Carola Universität, Heidelberg, 2023.

[72] T. Morgenroth, *S-EBIT commissioning*, Ph.D. thesis, Friedrich-Schiller-Universität Jena, 2024.

[73] M. Vogel, G. Birkl, M. Ebrahimi, D. von Lindenfels, A. Martin, G. Paulus, W. Quint, S. Ringleb, T. Stöhlker, and M. Wiesel, *Extreme-field physics in Penning traps: The ARTEMIS and HILITE experiments*, Hyperfine Interact. **236**, 65 (2015).

[74] S. Rausch, *Measurement data from commissioning of the HITRAP facility*, 10.48328/tudatalib-2001 (2025).